Vertex Detector Technology and Jet Flavour Identification at the Future e^+e^- Linear Collider

C J S Damerell and D J Jackson

Rutherford Appleton Laboratory, Chilton, Didcot, OX11 0QX, England

ABSTRACT

The future e^+e^- Linear Collider will offer unique opportunities for new physics, both within the Standard Model and for discoveries beyond the SM. In all these areas, access to the physics will depend on a detector providing high efficiency and purity for heavy flavour (charm as well as *b*) identification of all jets in the event. Building on the experience at SLC (the original and upgrade vertex detectors of SLD) we are designing a novel CCD-based detector which will be matched to these most challenging physics requirements. The secret of success will be very thin barrels with fine segmentation ($2500\ \text{pixels}/\text{mm}^2$). In this paper, we indicate in general how such a detector can be built, (including areas where R&D is needed) and we also make some preliminary calculations of the potential performance of the detector. The most important new result is the demonstration that highly efficient and pure *b* and charm jet identification can be achieved.

1. INTRODUCTION

The energy region to be covered by the future e^+e^- Linear Collider (hereafter referred to as LC, or JLC/NLC/TESLA for the KEK/SLAC/DESY designs) may be rich in new physics such as the production of Higgs bosons, SUSY particles and totally unexpected phenomena. Complex processes such as associated production of the SUSY Higgs particles *A* and *H* could lead to as many as 12 jets in the final state, with four of them *b* flavoured in this example. Even in the absence of new physics, the Standard Model processes (production of *WW*, *ZZ*, $t\bar{t}$, *WWZ*, etc) will be characterized by multi-jet topologies.

One of the great strengths of the e^+e^- production process has traditionally been our ability to perform whole-event analysis of the hadronic final states, with high efficiency. As $\sqrt{s}$ increases, this aim becomes more challenging for a number of reasons. Firstly, due to the increasing jet multiplicity, excellent hermeticity of the tracking and calorimeter system is essential, in order to avoid losing one or more of the jets. Secondly, excellent jet energy measurement is needed, in order to achieve adequate effective mass resolution for 2- or 3-jet systems. *W/Z* mass separation is essential, and one really wants to do much better than that, in order to optimize the signal-to-background in physics processes. Thirdly, high efficiency and purity for jet flavour identification is needed. Ideally, this means the clean separation of *b*, *c* and *udsg* jets. The information may be used for background suppression (in the case of background events of different flavour content from the signal), for reducing combinatorial background within an event (eg where only some fraction of the jets are *b* flavoured) and for measurement of branching ratios to differently flavoured final states (eg the ratio $(H \to c\bar{c})/(H \to b\bar{b})$ which can be crucial in distinguishing between models).

While a low level of tagging efficiency and purity may be compatible with some physics goals, it is clear that in many cases, particularly of discovery channels, one is likely to be faced with small signals, complex event structures, and high backgrounds which will conspire to place the most stringent demands on the flavour identification system. See [1] for a recent review of this topic. Our studies are driven by the concern for satisfying these physics aims, within the constraints set by other aspects of the collider/detector system. Specifically, our proposals for flavour ID avoid placing unrealistic demands on the final focus system in such areas as background control, and also avoid serious compromises in the jet energy resolution due to too thick a detector solenoid. However, these inter-system issues will need further study as the design advances, and some modest changes in the optimized parameters are to be expected.

As has been demonstrated in the SLD experiment, the key to achieving high quality flavour identification is a detection system which permits efficient topological reconstruction of the *b* and *c* vertices within jets. Due to the exponential decay distributions, high vertex finding efficiency implies the ability to recognise very short lived decays with respect to the parent vertex ie SV with respect to PV, or TV with respect to SV, where we use the nomenclature PV, SV and TV to denote the primary, secondary and tertiary vertices in a jet. To resolve a parent/daughter vertex combination, we need to measure the tracks with sufficient precision that most of them will be compatible only with their true vertex, the relevant figure of merit being the precision of measurement of the track at the interaction region (IR). In a well designed detector system, free of other constraints, this is determined by the track measurement precision in the innermost layer of the vertex detector (hereafter called Barrel 1 or B1), compounded by the effect of multiple scattering in B1, extrapolated to the IR. This optimal situation applies if the B2 radius is at least twice the B1 radius.

Thus the impact parameter precision for any track is given by two terms, a constant term that depends on the track measurement precision in each barrel, added in quadrature to a momentum dependent term given by the multiple scattering in

B1. For e^+e^- collisions leading to hadronic final states, both the jet multiplicity and the track multiplicity within a jet will on average increase with $\sqrt{s}$. Thus the mean momentum of charged tracks increases only very slowly, being around 2 GeV/c for $\sqrt{s}$ = 0.5 TeV. For this reason, the multiple scattering term is dominant in determining the impact parameter precision of most hadronic tracks in any vertex detector yet built or conceived for the e^+e^- collider environment. Efforts to thin the material of the beam-pipe and B1 are of course of great importance, but the gain factor is only as the *square root* of the thickness. More important in general are efforts to reduce *R* (B1), the inner barrel radius, leading *linearly* to improvements in the measurement accuracy at the IR. *Consequently, R* (B1) *is the overriding performance parameter in an optimized design.*

Optimizing the quality of the flavour tagging thus involves two parameters (track measurement precision and barrel thickness) which are intrinsic to the vertex detector, and one other (B1 radius) which is determined by external factors (notably background). In Section 2 of this paper, we explore ideas for minimizing *R* (B1) and in Section 3 we establish the goals for detector precision and thickness. Once these parameters are settled, we can determine the precision in track measurement at the interaction region. In Section 4 we describe the general procedure for using the measured tracks for topological vertex finding, and in Section 5 we evaluate the efficiency/purity for separating *b*, *c* and light quark jets, on the basis of their different vertex structures and kinematic properties. Finally in Section 6, we discuss future studies and R&D work needed to at least establish our aims, and maybe substantially improve on them, on the timescale of the future collider.

2. BACKGROUND AND RADIATION-DAMAGE ISSUES

Being closest to the beam-line, Barrel 1 of the vertex detector is the most susceptible element of the entire detector system, both as regards background and also radiation damage. Indeed, it is these considerations which determine the B1 radius; in the absence of background one would gain in performance by making it even smaller.

The effect of backgrounds can be minimized by optimal detector design as well as by reducing the intrinsic background levels. In the case of the vertex detector, both strategies are fully implemented. Regarding the detector design, the first concern is that of segmentation. As in SLD, the plan is to use CCD detectors with pixel sizes 20x20 μm^2. These dimensions are chosen to give adequate (~3.5 μm) spatial resolution by analogue readout and cluster centroid determination. This fine segmentation (2500 pixels/mm^2) leads incidentally to a high tolerance of background. Signal clusters remain cleanly isolated from the sea of background even up to levels of some tens of hits/mm^2.

The next issue for the detector design is the readout time. A CCD detector system can easily be made deadtimeless; subsequent events occurring during readout are accepted simply by extending the readout time. The reason to minimize the readout time is exclusively that of background reduction. By a combination of high speed readout and multi-port CCD architecture, one could achieve complete detector readout between bunch trains, so that the relevant background would be that accumulated during just one bunch train. However this would place a heavy requirement on the local electronics outside the cryostat, due to the need for processing the large number of readout channels in parallel. The background in Barrel 1 is (on our design) approximately ten times higher than in Barrel 2. Consequently, the system is designed to achieve readout within one bunch-train-interval (BTI) only for the innermost barrel; one can take advantage of the CCD analogue storage capability to reduce the number of readout channels needed for B2-B5. Reducing the number of channels also reduces the power dissipation inside the detector cryostat, permitting one to retain a gaseous cooling system. This is important, for if liquid cooling were needed, the detector thickness would inevitably be increased, degrading the physics capability.

As well as optimizing the detector design, much can be done to minimize the backgrounds seen by the vertex detector. These strategies are discussed in [2]; here we summarize the main conclusions. For the present SLD vertex detector, the most serious background is due to synchrotron radiation (SR) photons generated in the final focus triplet by each incoming beam bunch. These photons are able to strike material within ~2 m of the IP on the exit side, and thereafter (via double or triple scattering and fluorescence) to generate photons directed into the vertex detector and beyond. The lowest energy X-rays are absorbed by the stainless steel beam-pipe or (in the vertex region where the beam-pipe is beryllium) by a titanium liner. Above this cutoff, X-rays of progressively higher mean energy are absorbed in B1, B2, etc. The typical hit density from these X-rays is around 0.5/mm^2, which would be serious in a microstrip detector but is perfectly tolerable in a pixel-based system.

In the future LC, this source of background is effectively eliminated. By using a non-zero (20 mrad) crossing angle, and exit quadrupoles of larger aperture than the entrance quads, the primary SR sails through the interaction region, to be dumped safely many metres downstream. A small SR-related background remains in the NLC design, from the final doublet at $|z| \approx 150$ m, but this can be masked with high efficiency.

The potentially most serious background at the future LC is e^+e^- pairs generated by the beam-beam interaction. For the NLC parameters, the majority come from coherent interactions between beamstrahlung photons and electrons of the incoming bunch, the Bethe-Heitler process $\gamma e \to e^+e^-e$. While the pair electrons are produced at very small angles, they experience a transverse kick from the incoming beam which can deflect those with low energy into the aperture of the

vertex detector (which extends to $|\cos\theta| = 0.9$). Fortunately, these low energy electrons can be effectively confined to small radius by using a high field detector solenoid. For this reason, since 1993 (Hawaii Workshop [3]) it has been suggested to use a 4 Tesla solenoid for the future LC detector. This field value is somewhat arbitrary (higher would be even better!) but is believed to represent a reasonable compromise between the requirements of the vertex detector and the negative impact of a thick solenoid on the hadron calorimetry (the EM calorimeter will certainly be located inside the coil). Within the polar angle range $|\cos\theta| < 0.9$, the 4 T solenoid reduces the hit rate due to pair background to $< 4/\mathrm{mm}^2$ at B1 and to $< 0.4/\mathrm{mm}^2$ at B2 [4]. (All hit densities are quoted per bunch train.) The pair electrons are transported into the apertures of the conical masks. In the case of the NLC final focus, they then enter a nearly field-free region (due to the use of a compensating solenoid) before striking various surfaces within this aperture. A worst-case simulation (no compensating solenoid, electrons driven into the faces of the final focus quads) leads to relatively high fluxes of backscattered particles ($\sim 15/\mathrm{mm}^2$ at B1 and $\sim 2/\mathrm{mm}^2$ at B2) [4]. Studies for TESLA by D Schulte [5], indicate that by facing these quads with a low-Z (graphite) absorber, this rate can be reduced by an order of magnitude. By appropriate tuning of the residual field within the compensating solenoid, a further reduction can be made. In view of this, we anticipate that the backscattered particle background at B1 and beyond can be reduced below that due to the irreducible pair background, mentioned above. Hence the overall hit density in the VXD system (per bunch train) can be controlled to the level of $\sim 5/\mathrm{mm}^2$ (B1) and $0.5/\mathrm{mm}^2$ (B2), and much less in the outer barrels. Leisurely readout of most of the detector is thus permitted (eg 4 BTIs for B2), but B1 will be read (or cleared) completely between each bunch train.

As well as the effect of backgrounds on the detector occupancy, it is important to consider the associated radiation damage in the CCDs. As regards ionization effects, the predominant charged particle background (pair electrons) will also be the main cause of damage. This arises mostly as a result of electron-hole pair creation in the gate oxide, leading to fixed positive charge at the silicon/oxide interface. The associated flat-band voltage shifts can be compensated for by changes in bias voltages, but these are eventually limited by the maximum operating voltage of the output amplifier. Using standard production procedures, CCDs of the type proposed for this application are tolerant of ~100 krad of ionizing radiation. Using more advanced procedures, 1 Mrad-tolerant devices can be produced. For the calculated background in B1, we estimate that standard production devices would have a lifetime of six years (1 year = 10^7 seconds at full luminosity). Note that these backgrounds would be very much worse if the detector solenoid were not at full field; it is essential to interlock the beam delivery system with the solenoid once the radiation-sensitive detector elements are installed.

As well as the ionizing effects of radiation, CCDs are susceptible to damage by displacement of silicon atoms in the bulk crystalline material. The associated bulk traps result in charge-transfer inefficiency (CTI), which causes loss and smearing of signals from remote regions of the CCD. In the case of NLC, the effects of pair and backscattered electrons (as long as the solenoid is on) are minor. The main concern would be neutrons generated by the interaction of beamstrahlung photons, QSR photons and pair electrons, with material in the region of the detector. As with tolerance of ionizing radiation, limits can be quoted for standard devices and for optimized designs. Using current technology, a fluence of (or equivalent to, as regards non-ionizing energy loss NIEL) 3×10^9 neutrons/cm^2 of energy 1 MeV represents a conservative upper limit. Taking advantage of developments now underway [6], approximately an order of magnitude improvement may be expected on the NLC timescale. Neutron background estimates for NLC are now in progress. In the case of TESLA, preliminary indications [7] are that neutrons from the beamstrahlung dump would set a three year lifetime for CCDs of current design. This is clearly an area that needs to be watched carefully.

3. DETECTOR DESIGN

The general detector layout is shown in an isometric view in Fig. 1 and in cross-section in Fig. 2. The tapered beam-pipe is designed to accommodate the envelope of nearly all pair electrons, as discussed previously.

The general idea behind the 5-barrel (660 Mpixel) layout is as follows. While the B1 background is perfectly compatible with its use for track fitting, by including the on-track cluster to refine the measurement of impact parameter, the hit density would make it less readily usable in the pattern recognition. The intention is to achieve stand-alone track finding in the vertex detector using layers B2-B5. This provides a comfortable degree of redundancy. Found tracks are then extrapolated outward for linking to the Central Tracking Detector, and also extrapolated inwards for linking to B1 hits, prior to a global fitting and optimal determination of track parameters. Including B1 in this fit gives almost a factor of two improvement in the precision of the impact parameter at the IP (multiple scattering term).

The generous radial spacing between the barrels ($R(\mathrm{B2}) = 2\times R(\mathrm{B1})$; $R(\mathrm{B3}) = 3\times R(\mathrm{B1})$; etc) provides excellent impact parameter resolution, while retaining achievable CCD lengths even for Barrel 5. Note the use of single CCDs per ladder on B1 and B2, and two CCDs beyond.

The mechanical support structure (not shown in the drawing) will be similar to that used in the SLD vertex detector [8]. It will introduce negligible material into the vertex detector tracking region ($|\cos\theta| < 0.9$) but will hold the ladders rigidly at each end, providing excellent resistance to bowing; the intrinsic ladder flexibility would otherwise make them particularly susceptible to such distortions. The cryostat consists essentially of a foam shell with adequate thermal insulation characteristics, and thickness $\sim 0.5\%\ X_0$. This material, being outside the vertex detector, has a negligible

effect on the impact parameter precision. The detector is cooled to the operating temperature of around 180 K (chosen to minimize the effects of bulk radiation damage in the CCDs) by nitrogen gas.

The key to the detector performance is the design of the ladders; see Fig. 3. Each ladder consists essentially of a substrate (probably beryllium) which (in conjunction with the endplates of the support structure) provides the mechanical support for the CCDs. The CCDs are attached face-up to the ladder substrate. By a particular processing procedure [9] the CCDs can be thinned almost to the edge of the epitaxial layer (~30 μm overall thickness).

The CCDs on the 1-CCD ladders (B1 and B2) can be read out through each end, while those on the 2-CCD ladders are read only through the outer end. Thus (unlike the SLD detector) there is no need to route any electrical connections to the inner region of the ladder, hence permitting the absolutely minimal ladder thickness. The overall ladder (or barrel) thickness in the active vertex detector volume thus becomes 0.07% (substrate) + 0.02% (adhesive) + 0.03% (CCD), a total of 0.12% X_0. These thin barrels permit unprecedented performance capability; even for low momentum tracks, one is able to make effective use of the point measurement precision of the CCD, which is approximately 3.5 μm. Simulating the performance of the vertex detector, we obtain the following for the impact parameter measurement precision (in microns) for a track of momentum p GeV/c and polar angle θ :

$$\sigma_{XY} = \sigma_{RZ} = (4.5 - R/8) \oplus 5.5(1 - R/12)/(p\sin^{3/2}\theta)$$

where R is the radial distance from the IP at which the impact parameter is evaluated, in mm. Note that for decays that occur at a radial position which is a significant fraction of R (B1), the impact parameter precision at the vertex is considerably improved. For high energy jets, this leads to an enhancement in the fraction of secondary/tertiary vertices found.

Before evaluating the usefulness of such a detector for physics (Sections 4 and 5) we note a few unrelated technical issues. The inner section of beam-pipe (of radius 10 mm) is made of beryllium, followed by a transition to stainless steel for the conical section and beyond. By using thin walled stainless steel in the region where the beam-pipe penetrates the cryostat, the heat leak can be held down to a comfortable level.

The most difficult problem with the SLD front-end electronics (which eventually forced a reduction in the readout frequency from 10 to 5 MHz) was crosstalk between the clock pulses of the CCD readout register and the analogue signal output. Since the majority of the crosstalk was taking place at

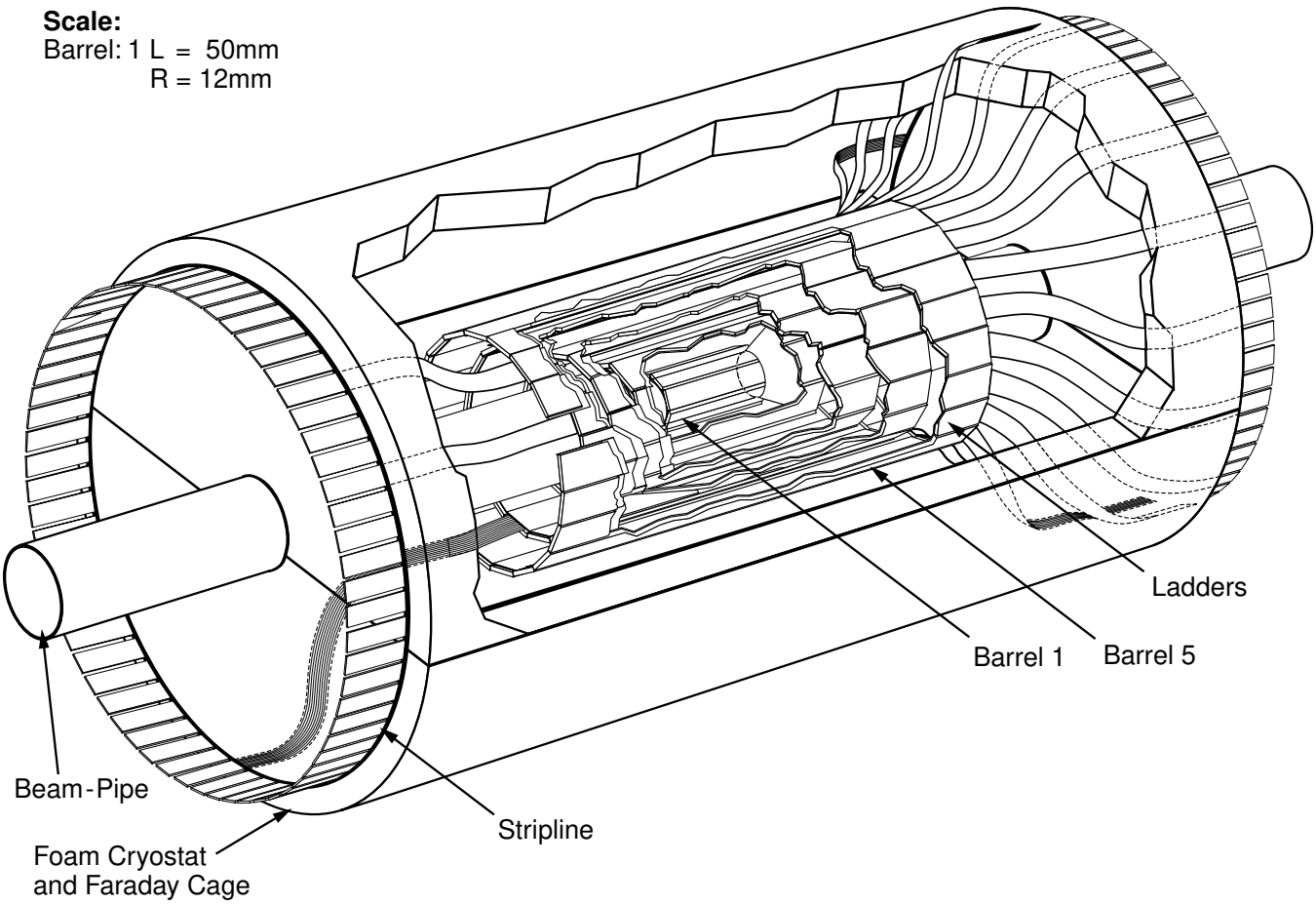

Fig. 1 Cut-away isometric drawing of the suggested 5-barrel vertex detector. All non-CCD electronics is external to the cryostat, in the small angle region below the limit of tracking.

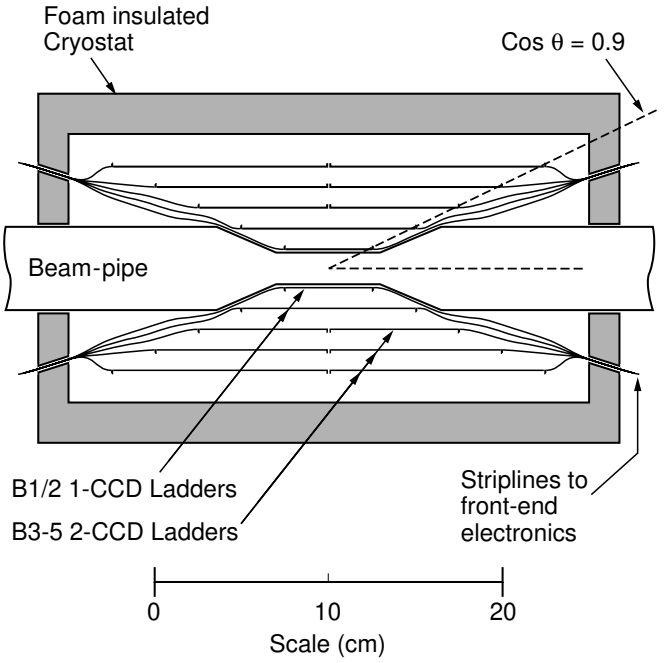

Fig. 2 Cross-section of the suggested vertex detector.

the front-end electronics board (just outside the cryostat) or on the stripline connection between that board and the ladder, a very attractive solution for the future LC will be to generate the high current fast register drive pulses on or adjacent to the CCD chip, greatly reducing the level of crosstalk. Then it is reasonable to expect that the HDTV-like clocking rate of 50 MHz will be achievable with low clocking-related noise. The intrinsic noise performance of the CCD output amplifier can certainly be reduced to below 100 e^- RMS at 50 MHz sample frequency [10] (using correlated double sampling between successive pixels). We can then expect to read out the background-critical Barrel 1 within one bunch train interval (BTI), the much quieter outer barrels within a sufficiently small number of BTIs, and all this with a modest number of output channels (384, comparable to that of the SLD detector), see Table 1. With this arrangement, the front end electronics can be accommodated within a small polar angle range (probably inside the 65-100 mrad region shadowed by the conical masks). Moving the drivers adjacent to the CCDs will increase the power dissipation inside the cryostat. This has to be studied in detail, but there are ideas for doing this with a

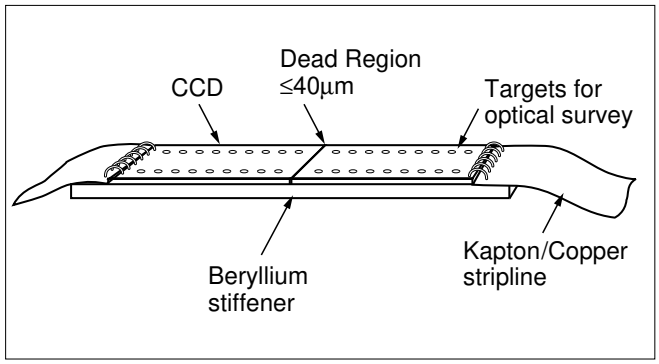

Fig. 3 Advanced 2-CCD ladder design. Active length 5-25 cm. Shorter ladders used for B1 and B2 will be built with only one CCD, read out from both ends.

relatively small increment in the baseline dissipation (~20 W), so that the low mass gaseous cooling can be retained.

4. TOPOLOGICAL VERTEXING

Using the SLD algorithm for topological vertex reconstruction, we compare jet flavour tagging with the original SLD vertex detector VXD2, the upgrade VXD3 and the proposed LC design. The specifications of the vertex detector that determine the tracking resolution have been discussed in Section 1. The uncertainty of the position of a track extrapolated back to the e^+e^- interaction point (IP) for the three detectors is listed in Table 2. The table shows the constant $\oplus$ multiple scattering terms for both the *XY* and *Z* track projections.

Since the CCD pixel detector locates the track in both of these projections, the probability of misassigning a track to a spatial point (eg the IP or a decay vertex) grows as the *square* of the detector resolution. Hence the efficiency of the 3-D topological vertex algorithm described below improves significantly with improved vertex detector resolution.

In order to study the flavour tagging performance, the SLD $e^+e^- \to Z^0$ Monte Carlo is used. Stable charged MC tracks from the hadronic Z^0 decays are selected with $|\cos\theta| < 0.9$ and transverse momentum wrt the beam exceeding 250 MeV/c. After finding jets from this set of tracks, events with more than two jets are rejected in order that a sample of ~45 GeV jets is obtained. The MC tracks are smeared by the resolution given in Table 2 for each of the

Table 1 Parameters of CCDs and ladders. For each barrel, R = barrel radius, L = ladder length, W = ladder width

Barrel	R mm	L/2 mm	W mm	CCDs/ Ladder	CCD size (MPix)	Outputs/ CCD	Ladders	Read Time ms	Hit Density mm^{-2}
1	12	25	12	1	1.5	12	8	4.5	5
2	24	50	24	1	6.0	12	8	18	0.5
3	36	75	24	2	4.5	2	12	40	0.2
4	48	100	24	2	6.0	2	16	54	0.15
5	60	125	24	2	7.5	2	20	67	0.1

Table 2 Track impact parameter resolution transverse σ_{XY} and longitudinal σ_Z to the beam; $s = 1/p\sin^{3/2}\theta$, where p is the particle momentum in GeV/c and θ is its polar angle.

	$\sigma_{XY}(\mu\text{m})$	$\sigma_Z(\mu\text{m})$
VXD2	$11 \oplus 70s$	$38 \oplus 70s$
VXD3	$9 \oplus 29s$	$14 \oplus 29s$
LC	$4.5 \oplus 5.5s$	$4.5 \oplus 5.5s$

three vertex detectors, to produce three MC sets from the same initial sample of 28,000 jets. The MC location of the IP, used in the topological vertex algorithm, is also smeared by an appropriate amount $\sigma_{XY} = 7$ μm and $\sigma_Z = 50$ μm for SLD, $\sigma_{XY} = 4$ μm and $\sigma_Z = 10$ μm for the LC). The jets are divided into three categories, the heavy quark *b*-jets and *c*-jets and the light quark *uds*-jets.

The topological vertex reconstruction is applied separately to the tracks in each jet. The algorithm is described in detail in [11] and summarized here. The vertices are reconstructed in 3-D co-ordinate space by defining a vertex probability $V(\mathbf{r})$ at each position $\mathbf{r}$. The helix parameters for each track i are used to describe the 3-D track trajectory as a Gaussian tube $f_i(\mathbf{r})$ where the width of the tube is the uncertainty in the measured track location close to the IP (Table 2). $V(\mathbf{r})$ is defined as a function of the $f_i(\mathbf{r})$ such that it is sensitive to the track multiplicity at $\mathbf{r}$ and is small in regions where less than two tracks (required for a vertex) have significant $f_i(\mathbf{r})$. An example of these functions for VXD2 with a MC *b*-jet is represented in Fig. 4.

A further function $f_0(\mathbf{r})$ is used to describe the location and uncertainty of the IP. This function is combined with the $f_i(\mathbf{r})$ in the definition of $V(\mathbf{r})$ in order to later identify the tracks forming the PV. Maxima are found in $V(\mathbf{r})$ and clustered into spatial regions using the criterion that two maxima are resolved if the value of $V(\mathbf{r})$ on a straight line between the maxima falls below 60% of the value of $V(\mathbf{r})$ at either maximum. In Fig. 4(b), a SV is resolved from the PV at $x = y = 0$. Tracks are associated with these resolved regions to form a set of topological vertices. Non-primary vertices are labelled as secondary (SV) or tertiary (TV) etc according to their relative distance from the PV.

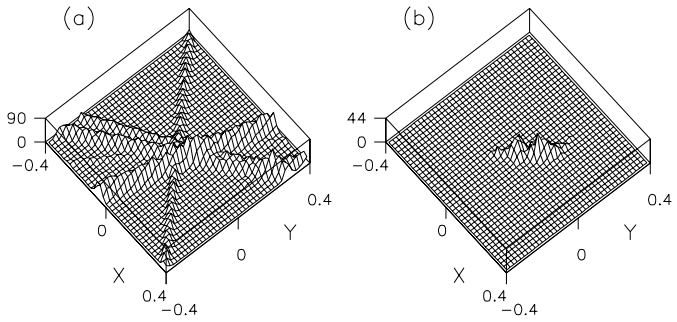

Fig. 4 The functions (a) $\sum f_i(\mathbf{r})$ and (b) $V(\mathbf{r})$ integrated over z and projected onto the XY plane (cm)

Table 3 Classification of reconstructed vertex topologies (%) for the LC vertex detector (with SLD VXD2 performance shown in parentheses).

	b-jet	*c*-jet	*uds*-jets
PV only	20.0 (45)	50.4 (85)	99.1 (99)
PV + SV	53.5 (50)	48.7 (15)	0.8 (1)
PV + SV + TV	25.7 (5)	0.9	0.1
>TV	0.8	0.0	0.0

For flavour tagging, the furthest vertex from the PV is rejected if it is consistent with a $K^0 \to \pi^+\pi^-$ decay, since such vertices are background to the signal *B* and *D* hadron decay vertices. The classification of vertex topologies is shown in Table 3 for the LC. The ideal case would be to identify the PV for all jets together with a *D* decay SV for *c*-jets, or a *B* decay SV plus *D* decay TV for *b*-jets. As expected, there is a considerable improvement in the efficiency to fully reconstruct the decay sequence by a factor of five for *b*-jets and three for *c*-jets due to the detector upgrade from VXD2 to the LC.

The efficiency for topological classification is limited by the detector resolution, given the short *B* and *D* hadron lifetimes, and ultimately by decays with low charged track multiplicity, since at least two such tracks are required to find the vertex.

5. JET FLAVOUR IDENTIFICATION

While different topologies could be used for jet flavour tagging at the LC, it is the kinematic differences between vertices in the jets of the three flavour categories that is exploited by the SLD tag and used here. This *b*-tag utilizes the mass difference of the *B* and *D* hadrons (~5 GeV and ~2 GeV respectively) in forming the main tag variable. For this procedure, the categories with and without tertiary vertices are combined, by defining a 'seed' vertex as the furthest vertex from the PV. The efficiency of the mass tag relies on the ability to identify tracks with the heavy flavour decay. As discussed above, some branching fractions (eg semileptonic decays) produce only one track at a decay vertex. Thus further tracks are attached to the seed vertex using a procedure described in [11].

The invariant mass M of the tracks either in the seed vertex or attached to it, is calculated assuming the pion mass for each track. The transverse component p_T of the total momentum of these tracks relative to the vertex axis (the line joining the IP to the seed) is calculated in order to determine the 'p_T added mass'.

$$M_{p_T} = \sqrt{M^2 + p_T^2} + |\, p_T \,| \qquad (1)$$

This quantity is the minimum mass the decaying hadron could have in order to produce a vertex with the quantities M and p_T. The direction of the vertex axis is varied

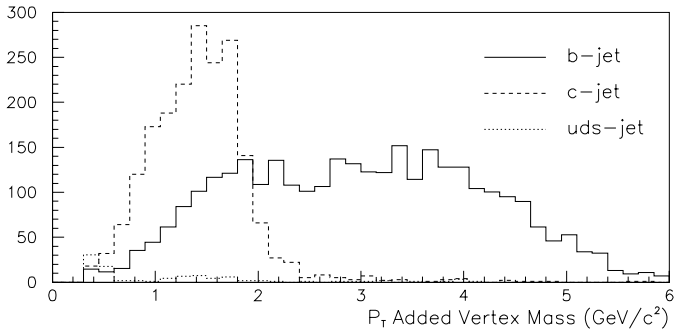

Fig. 5 Jet flavour dependence of the M_{p_T} distribution for LC detector.

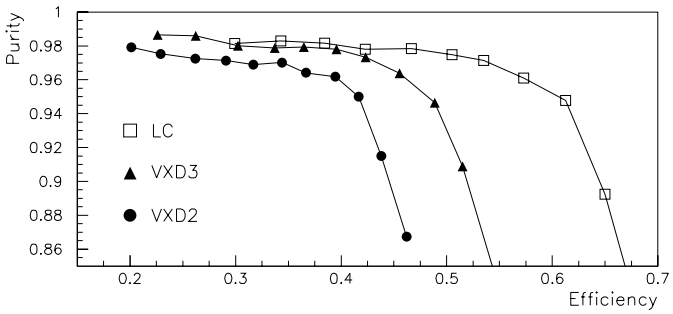

Fig. 6 Performance of *b*-jet flavour tag.

within the one-sigma limits constraining the axis at the measured IP and reconstructed seed vertex such that the p_T is minimized within this variation. This procedure prevents non-*B* background vertices acquiring a high value of M_{p_T} due to a small fluctuation in the measured vertex axis direction. Accurate 3-D vertexing and a precisely measured IP allow significant gain in the *b*-tag efficiency with high purity using this technique [12]. The mass tag variable, reconstructed with the LC detector, is shown in Fig. 5. Here, and in the following, the events are normalized to equal numbers of generated jets of all five flavours *udscb*.

The b-jets are tagged by a cut on M_{p_T}. Fig. 6 shows the purity against total efficiency $\varepsilon_{b\text{-jet}}$, for b-jets obtained by varying this cut from $M_{p_T} > 1.6$ GeV to $M_{p_T} > 3.6$ GeV for the three vertex detectors considered. Many physics applications rely on the ability to tag n jets, with $n > 1$, for which the event efficiency is proportional to ε^n_{b-jet}. Fig. 6 demonstrates that there is a significant dependence of $\varepsilon_{b\text{-jet}}$, and hence the physics potential of the LC, on the vertex detector resolution.

It should be noted that *b*-tags based only on track impact parameters to the IP do *not* improve significantly with the detector resolution. Using such tags, with improving vertex detector resolution the *c*-jet efficiency begins to increase faster than any further increase in *b*-jet efficiency, degrading the purity of the *b*-jets. The improved resolution also allows more efficient topological vertex reconstruction, again for both *b*-jets and *c*-jets (Table 3), however, having identified the tracks from the heavy hadron decays the mass tag retains the *b*-jet purity due to the sharp kinematic cut-off for charm at 2 GeV, as shown in Fig. 5.

For the LC detector the vertex reconstruction is efficient enough to use the same procedure to tag c-jets with a cut on M_{p_T} below ~2.0 GeV. There are a number of additional factors that distinguish the two heavy quark jets such as vertex momentum, vertex decay length and neutral energy in the calorimeter in line with the vertex axis. These quantities remain to be studied further. Another feature, the vertex fit probability, is used here to improve the *c*-jet purity. Since the vertex tracks in a *b*-jet originate at two decay points the probability of the fit to a single vertex is expected to be lower than for the *c*-jet vertices. A 'vertex' here refers to the tracks in the seed together with the attached tracks. It is required that this probability is greater than 1%, and also that $M_{p_T} > 0.5$ GeV since the *uds* background peaks at low mass. The resulting purity against total efficiency curves for the *c*-jets obtained by varying the cut from $M_{p_T} < 1.0$ GeV to $M_{p_T} < 3.0$ GeV is shown in Fig. 7; again comparison is made between the three detector designs.

The main reason for the relatively low vertex finding efficiency for *c*-jets is the low multiplicity of charged tracks from the *D* decay. By considering the topology consisting of a single track isolated from the PV in jets with no SV the efficiency may be enhanced. (This is similar to attaching the 1-prong tracks to the seed vertex to enhance the *b*-jet efficiency.) For the LC this PV+track topology is identified for 24.4% of *c*-jets compared with backgrounds of 7.2% (6.6%) in *b(uds)*-jets. The main source of the *uds* background is $K^0_s \to \pi^+\pi^-$ decays in which one pion is consistent with the PV and the other is isolated from it. Assuming that this contribution from *uds* events is removable, the fourth curve in Fig. 7 (labelled '2nd tag') shows the enhancement obtained by adding the PV+track topology to the events passing the reconstructed mass cut. (This curve is shown for the LC only, for VXD2 and VXD3 a similar relative improvement in efficiency for constant purity is observed.)

The main conclusion of this study is that the heavy quark jet tagging performance is strongly dependent on the vertex detector resolution. Table 4 summarizes this performance by listing the efficiencies for the signal and background jets for one point on each of the three purity-efficiency curves shown for the LC. The lst (2nd) *c*-tag refers to the tag without (with) the addition of the PV+track topology.

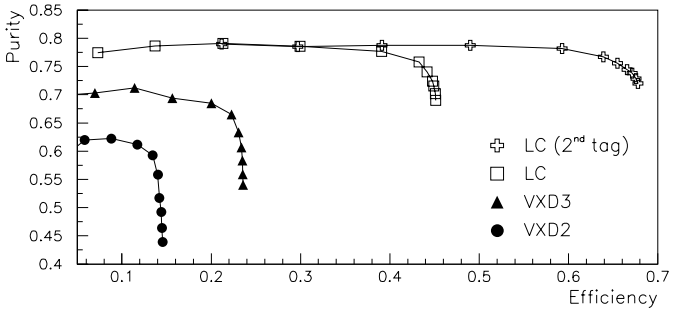

Fig. 7 Performance of *c*-jet flavour tag.

Table 4 Jet flavour tag efficiencies (%)

	b-jet	*c*-jet	*uds*-jets
b-tag	60.0	2.6	0.1
1st *c*-tag	11.0	40.0	0.2
2nd *c*-tag	18.1	64.4	<<6.6

6. FUTURE WORK

The original SLD detector was built by a small group over a period of eight years (six years of intensive R&D and two years of construction). The SLD upgrade detector, built by a much larger group, occupied only two years despite the use of fully custom-designed CCDs. However in this case, significant compromises were required (notably as regards the readout rate) in order to meet the schedule.

The detector for the future linear collider will require extensive R&D in a number of areas. For the CCDs themselves, the main challenges will be enhanced radiation hardness (with respect to displacement damage), enhanced performance of the output amplifiers (noise/bandwidth) and on-chip or local register drivers having very good decoupling with respect to the output amplifiers. The multi-port outputs have already been developed for other applications.

The experimental basis for the ladder design is the successful use of back-thinned, back-illuminated CCDs in astronomy. However, our substrates are much more flimsy, and probably imply a significant thermal expansion mismatch. The concept of stabilizing rather flexible ladders by attaching them firmly to a rigid support structure at each end is well established by the two SLD detectors. However, the future ladders will probably test this principle even more severely, and the overall assemblies will need careful study on temperature cycling.

Overall, the performance enhancements described in this paper will not be achieved without considerable effort. The cost of these developments will be minor, on the scale of the future machine, whereas the cost benefits will be enormous. What is most important is to assemble the collaboration to begin this work early enough that one can eventually construct the detector we need, not some rushed compromise system. Based on previous experience a good team effort over a period of 5-8 years should suffice.

The work described in this paper represents very much a first step in demonstrating the power of this novel detector as a tool for physics. The procedure we have described for flavour identification is open to considerable development. One can firstly make better use of the information already available (separate treatment of jets where a tertiary vertex is found, use of summed momentum of decay tracks, etc). One may also profit by invoking new information from other parts of the detector (eg π^0 gammas in the E-cal, or K_L^0 seen in the H-cal, which match to missing p_T from a decay vertex). In addition, future work will include a study of these tags as a function of jet momentum and their application to specific physics processes in the high energy e^+e^- environment.

It will also be important to investigate some of the design parameters which impinge significantly on other parts of the accelerator/detector system such as the magnitude of the solenoid field, and the Barrel 1 radius. However, as with previous vertex detectors at colliders, it is clear that even this design falls short of the asymptotic performance limits as regards flavour identification. Therefore, the discovery potential of the future linear collider, while greatly enhanced by this proposed detector, could be even better. Thus the only reason to relax on the external parameters mentioned above would be if achieving them placed unrealistic demands on some aspects of the machine design (eg the background control in the final focus) or seriously compromised other parts of the detector (eg the performance of the hadron calorimeter behind the coil). At present, no such problems are envisaged, though the machine backgrounds will surely take time to control to the required level. In any case, the prospects for physics at the future linear collider are apparently quite complementary to those at LHC, where the possibilities for vertex detection at full luminosity are much more limited. The goals outlined in this report appear to be quite realistic and are certainly well worth working towards; achieving them may well be rewarded by major discoveries to which the detector would otherwise be blind.

ACKNOWLEDGEMENTS

We wish to acknowledge the suggestions from many physicists and engineers working on SLD, JLC, NLC and TESLA who have contributed to these studies. We look forward to working closely with them in the intercontinental R&D programme for the vertex detector at the future LC, wherever it is built.

REFERENCES

1. K. Fujii, *Places Where VTX Will be Essential At Future Linear e^+e^- Colliders*, KEK Note, October 1995.
2. S.S. Hertzbach, T.W. Markiewicz, T. Maruyama and R. Messner, *Backgrounds at the Next Linear Collider*, proceedings of this Workshop.
3. C.K. Bowdey and C.J.S. Damerell, in *Physics and Experiments with Linear e^+e^- Colliders* (World Scientific) (1993).
4. SLAC Report 474 (1996) 841.
5. D. Schulte. Draft of PhD Thesis (DESY) (1996).
6. S. Watts, A. Holmes-Siedle and A. Holland, ESTEC Report BRUCRD-ESACCD-95-1R (1995).
7. D. Schulte (Private Communication).
8. SLD Collaboration, *Design and Performance of the SLD Vertex Detector*. To be submitted to Nucl. Instr. and Meth.
9. P. Pool (Private Communication).
10. *CCD32 Sensor Design Specification* (EEV Report) (1994).
11. D.J. Jackson, SLAC-PUB-7215 (1996) Nucl. Instr. and Meth, (to be published).
12. SLD Collaboration, SLAC-PUB-7170 (1996).